Point-contact spectroscopy of the electron-phonon interaction in palladium

1991 J. Phys.: Condens. Matter 3 6523

(http://iopscience.iop.org/0953-8984/3/33/026)

J. Phys.: Condens. Matter 3 (1991) 6523–6530. Printed in the UK

Point-contact spectroscopy of the electron–phonon interaction in palladium

V N Antonov†¶, A V Zhalko-Titarenko‡, V Yu Milman§, A V Khotkevich‖ and S N Krainyukov‖

† Max-Planck-Institut für Festkörperforschung, D–7000 Stuttgart 80, Federal Republic of Germany

‡ Institute of Metal Physics, Ukrainian Academy of Sciences, 36 Vernadsky str., Kiev 252142, USSR

§ University of Cambridge, Cavendish Laboratory, Madingley Road, Cambridge CB3 0HE, UK

‖ Institute for Low Temperature Physics and Engineering, Ukrainian Academy of Sciences, Kharkov, USSR

Received 28 August 1990, in final form 15 May 1991

Abstract. Results are reported of the experimental point-contact spectroscopy and of the theoretical investigation of the electron–phonon interaction (EPI) in palladium. It is shown that positions of the peaks in the point-contact spectral function are determined by the structure of the phonon spectrum, while their relative intensities depend on the Fermi surface topology and EPI anisotropy.

1. Introduction

This paper completes a series of publications [1–4] devoted to the investigation of phonon spectra and the electron–phonon interaction (EPI) in FCC platinum group metals (Pt, Ir, Rh and Pd). In palladium these properties have been previously studied both experimentally and theoretically [5–9], and model calculations of the phonon spectrum (see references in [10]) gave reasonable agreement with experiment [5]. Nevertheless the resolution achieved in the measurement of the point-contact EPI spectra in palladium [8, 9] was unsatisfactory. Hence further experimental investigation of the EPI in palladium is desirable combined with the theoretical study of the different factors contributing to the point-contact spectral function.

Previously a simple model for the transition-metal binding energy was proposed [11] in a framework of the pseudopotential approach. This model was used successfully in calculations of the phonon frequencies, equation of state, temperature dependence of the lattice heat capacity and the macroscopic Grüneisen parameter for ten FCC transition metals [2, 4, 11–13]. Phonon spectra were predicted in this model and used in the theoretical analysis of the EPI for iridium [3] and rhodium [4]. However, none of the FCC transition metals has been studied in such detail as palladium has as far as lattice dynamics is concerned. Hence the investigation of palladium not only enables some light to be shed on the nature of electron–phonon interaction in this

¶ Permanent address: Institute of Metal Physics, Kiev 252142, USSR.

0953-8984/91/336523+08$03.50

metal, but also a comparison of the accuracy of the phonon spectrum obtained using the pseudopotential model [11] to be made with that of other theoretical models.

The main subject of this paper is the study of the EPI in Pd, and the first section is therefore devoted to calculating the phonon spectrum which represents an important part of our work. The following sections are concerned with experimental and theoretical EPI spectral functions.

2. Theoretical phonon spectrum

The transition-metal binding energy model which is used in the present study was described in detail in [11, 12]. We shall only mention here that we use: (i) the local pseudopotential of the Animalu–Heine–Abarenkov type; (ii) the screening function due to Taylor; and (iii) the short-range pair potential which simulated the d–d interaction, exactly in the same form as in [11]. The parameters of the short-range potential and of the pseudopotential were determined by least-squares fitting of the elastic constants at equilibrium volume and they are given in [12]. We used the value of effective valence for nearly free electrons, $Z = 1.6$, derived from our band structure calculation [14].

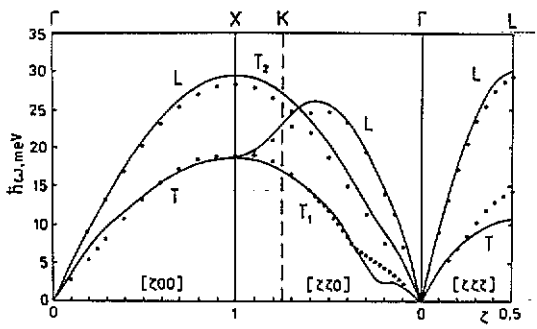

Figure 1. Phonon dispersion curves: full curve, present calculation; points, experimental data from thermal neutron scattering [5].

The calculated dispersion curves are shown in figure 1 together with the experimental data. The overall agreement between these two sets of frequencies may be considered as satisfactory and it is in fact better than in [15–17] for phonons both at the Brillouin zone face and at intermediate wavevectors. The transverse branch in the [111] direction presents an exception since the maximum frequency is underestimated by 17%. This disagreement is possibly due to the oversimplified form of the short-range potential used in this study (the Born–Mayer form of the potential). Our calculation confirms an experimental finding [5] that the phonon anomaly in the T_1 [110] branch at $\zeta \approx 0.25$ is of the Kohn type. The theoretical position of this anomaly does not coincide precisely with the measured value but we were able to show that, for example, the shift of this anomaly due to the alloying of Pd is described qualitatively correctly in this model [13]. Fortunately it is not necessary to describe this low-frequency feature of the phonon spectrum with high numerical accuracy in order to investigate the EPI spectral function. It will be shown in section 4 that the corresponding energy range gives a negligible contribution to the properties under consideration due to the geometric form factor of point-contact spectroscopy (structure factor of narrowing).

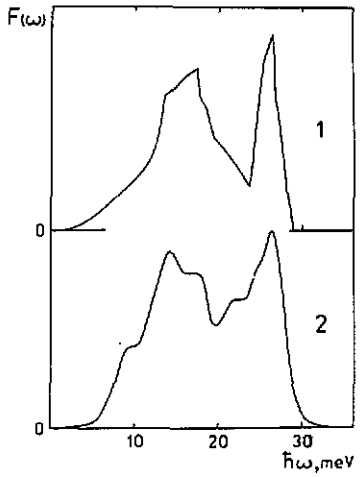

Figure 2. Phonon densities of states: 1, calculated in [5] using the force constants model; 2, present calculation.

The calculated phonon spectral density $F(\omega)$ is given in figure 2. This function and all other theoretical spectral densities described in the next sections were computed on a mesh with the step, $\Delta\omega$, equal to 0.05 meV and subsequently they were convoluted with the Lorentz function of 0.2 meV half-width in order to simplify comparison of the theoretical and experimental curves. Our result is in qualitative agreement with the calculation performed using the force constants model [5], as the main features are similar in both curves as shown in figure 2. Underestimation of the frequency of the T[111] branch mentioned earlier causes distortion of the low-frequency maximum in the phonon spectral density. However, the positions of the main peaks and the other features of this function at 13.6, 19.0 and 21.8 meV coincide with the measured values (see table 1). We conclude here that the pseudopotential model gives a reasonable description of the lattice dynamics of palladium and enables us to use computed phonon spectra in the theoretical study of EPI.

Table 1. The main features of the measured point-contact spectrum $g_{pc}(\omega)$ and calculated phonon density of states (frequencies in meV).

	ω_{max}	ω_T	ω_L	$\langle\omega\rangle$
$g_{pc}(\omega)$	30.3	16.0 ∓ 0.1	26.4 ∓ 0.3	12.82 ∓ 0.16
$F(\omega)$	29.9	14.8	26.7	18.83

3. Experimental study of EPI

The experimental study of the EPI in palladium was performed using point-contact spectroscopy [18]. We implemented sliding-type contacts created by shear force applied between two electrodes. The technique for measuring the point-contact EPI spectral function, $g_{pc}(\omega)$, is described elsewhere [1, 18]. Point-contact EPI spectra, i.e. the second harmonic of the modulating signal $V_2(V) \propto d^2V/dI^2(V)$, were obtained at

$T = 1.5$ K for 38 contacts. Typical experimental point-contact EPI spectra had two maxima and a shoulder near 7 meV. Unlike the well known results obtained for needle–anvil contacts under compressive force [9] we succeeded in obtaining spectra with an initial flat part without any zero anomalies caused by the deformation of the metal in the contact region which were always present in the experimental curves in [9]. Better spectral resolution than in [9] was achieved here due to a sufficiently lower level of modulating signal. As a result we were able to observe with confidence an additional feature of the spectrum between the two main peaks (at approximately 23 meV). The function $g_{pc}(\omega)$ reconstructed from the experimental spectra is given in figure 3. The main peaks of this function obtained in the present work are narrower than in [8, 9] due to better energy resolution. The location of the two main peaks and the mean phonon frequency which were obtained by averaging over 10 $g_{pc}(\omega)$ functions are given in table 1. The largest, and hence the most reliable [18], values of the electron–phonon coupling constant are equal to 0.23 and 0.34 with the point-contact background evaluated according to [19] and [20], respectively. We always observed a relatively high level of point-contact background in our study of palladium contacts. This effect is believed to be due to the electron–paramagnon interaction as in the case of platinum [1].

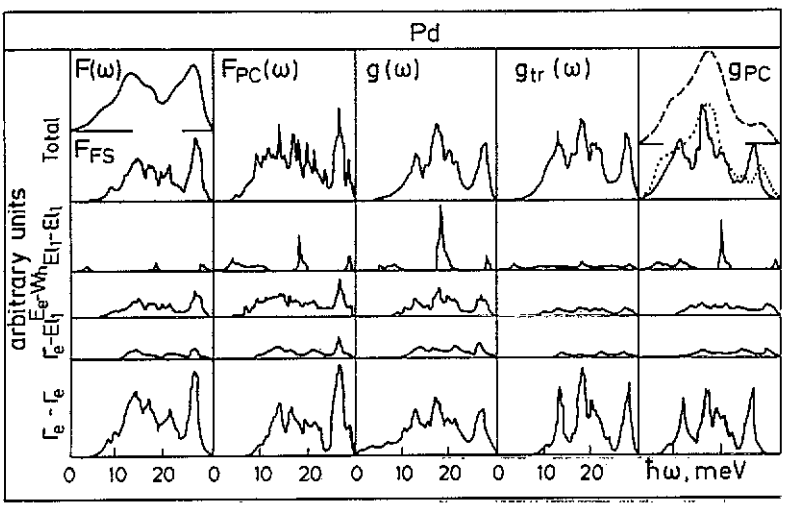

Figure 3. Spectral functions of the EPI and partial contributions from different scattering processes: full curve, present theoretical results; broken line, experimental point-contact spectrum from [9]; dotted curve, present experimental point-contact spectrum.

4. Theoretical calculation of EPI spectral functions

The point-contact EPI spectral function for a metal with an anisotropic Fermi surface (FS) may be evaluated from the following double integral over FS [18]:

$$g_{pc}(\omega) = \frac{\Omega_0^2}{(2\pi)^6} N^{-1}(E_F) \sum_{\nu nn'} \int \int_{FS} \frac{dS_n \, dS'_{n'}}{|v_k||v_{k'}|} |M^{\nu}_{kk'}|^2 K(k,k') \delta(\omega - \omega^{\nu}(k - k')) \qquad (1)$$

where Ω_0 is the volume of the Wigner–Seitz cell, $N(E_F)$ is the density of electronic states at the Fermi level, v_k is the velocity of electron at the Fermi surface, $\omega^\nu(\boldsymbol{k}-\boldsymbol{k}')$ is the phonon frequency of the νth branch (atomic units are used in (1)). We use $\boldsymbol{k}$ as a shorthand for the wavevector, $\boldsymbol{k}$, and the band index, n. The summation in (1) is over the Fermi surface sheets n, n' and over the phonon branches. The factor $M^\nu_{kk'}$ is the matrix element which corresponds to the scattering of an electron from state $\boldsymbol{k}$ to state $\boldsymbol{k}'$ by absorption or emission of a phonon of a branch ν. The structure factor of narrowing, $K(\boldsymbol{k},\boldsymbol{k}')$, depends on the wavevectors, $\boldsymbol{k}$ and $\boldsymbol{k}'$, of the electron states which contribute to the electric current in the point contact. This factor takes into account the influence of the geometry of the microcontact on the efficiency of the electron scattering in the spatial region of this contact. We used in our calculations the clean limit approximation for the circular hole [21]. The technique for computation of $g_{pc}(\omega)$ was developed in [6] and in other papers by these authors. In the present work we use the generalization of this method which takes relativistic effects into account [22].

The difference between $g_{pc}(\omega)$ and $F(\omega)$ is determined by a number of factors, i.e. by the structure factor of narrowing, the EPI matrix element and the topology of the Fermi surface. Elimination of the $K(\boldsymbol{k},\boldsymbol{k}')$ from equation (1) transforms $g_{pc}(\omega)$ into the Eliashberg function $g(\omega)$ (also known as $\alpha^2F(\omega)$). Further elimination of the EPI matrix element from $g(\omega)$ gives a new function, $F_{FS}(\omega)$, introduced previously in [1, 3]. The difference between $F_{FS}(\omega)$ and the spectral phonon density, $F(\omega)$, is determined by the FS topology. Using the constant matrix element in the evaluation of the integral in (1) one can study the influence of the structure factor of narrowing only (function $F_{pc}(\omega)$ from [4]).

The calculated Eliashberg spectral function, $g(\omega)$, is given in figure 4 in comparison with the previous theoretical data [9, 23]. Reasonable agreement between different calculations is observed with respect to peak positions and relative magnitude. Other spectral functions of the EPI are shown in figure 3. We used the FS obtained in [24] using RAPW calculation, and the FS topology compares well with previous results of Andersen [25].

It may be shown from our results that the EPI in palladium is determined mainly by intersheet scattering on the electronic surface in the Brillouin zone centre (Γ_e) as in the case of platinum [1]. This seems to be explained by the greater surface area of this sheet of the FS with respect to the hole monster (W_h) and to the ellipsoid at the X point (EL_1) which leads to the dominant Γ_e–Γ_e scattering contribution to $F_{FS}(\omega)$, $F_{pc}(\omega)$ and hence to all other EPI spectral functions. The topology of the Fermi surface has a relatively small influence on the phonon efficiency in EPI as follows from the fact that the difference between $F_{FS}(\omega)$ and $F(\omega)$ is less than for other platinum group metals [1, 3, 4].

It is interesting to note that whereas the EL_1–EL_1 scattering is less efficient from the point of view of weighting factors for the corresponding scattering wavevectors (see $F_{FS}(\omega)$ in figure 3), the contribution of this process to $g(\omega)$ is sharply enhanced due to the EPI matrix element, so the main peak of $g(\omega)$ becomes more intensive due to the EL_1–EL_1 scattering. Taking the EPI matrix element into account leads to redistribution of the peak intensities in the 10–20 meV range and to suppression of the contribution from phonons with frequencies less than 15 meV. The Eliashberg EPI function for Γ_e–Γ_e scattering has a peak at 23 meV apart from peculiarities at 12 and 17 meV. This feature is revealed in the total $g(\omega)$ function while it is absent in the $g(\omega)$ obtained in a non-relativistic approach [6]. Manifestation of this feature

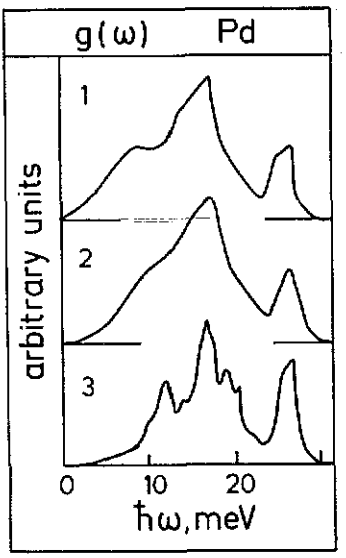

Figure 4. Calculated Eliashberg function for Pd: 1, from [23]; 2, from [9]; 3, present calculation.

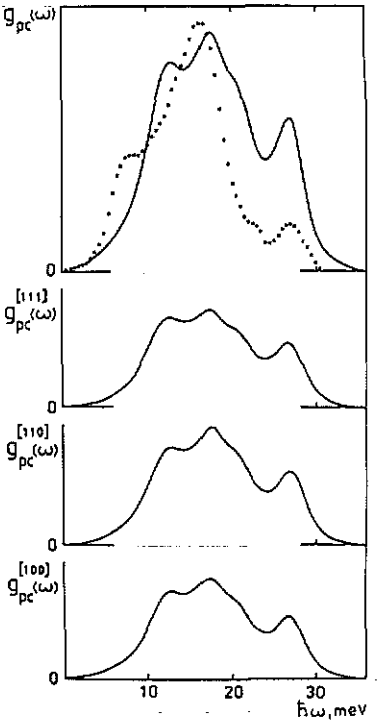

Figure 5. Calculated anisotropy of point-contact EPI function for the main crystallographic directions. The points, $g_{pc}(\omega)$, are reconstructed from our experimental data.

in our calculation seems to be connected with the essential influence of spin–orbit interaction on the palladium FS, hence we expect that the $F_{FS}(\omega)$ functions obtained in the relativistic [24] and non-relativistic approach [7] should also differ.

The structure factor of narrowing mainly affects the low-energy part of the spectrum, lowering in fact contribution from phonons with frequencies less than 7 meV to zero (compare $F_{FS}(\omega)$ and $F_{pc}(\omega)$ in figure 3). This factor also changes the relative importance of the different scattering processes for the point-contact spectrum compared with the Eliashberg function. The contribution from the EL–EL scattering is enhanced by taking into account the structure factor of narrowing, and the W_h–W_h scattering, which is not important for the $g(\omega)$ function, contributes substantially to the efficiency of phonons responsible for the formation of the EPI point-contact function.

The function $g_{pc}(\omega)$ is mainly determined by Γ_e–Γ_e scattering, the peaks of the phonon spectral density at 13 and 17 meV becoming narrower due to suppression of the 15 meV phonons caused by the anisotropy of EPI matrix element. When one takes into account the EPI matrix element the contribution from intra-ellipsoid scattering to the total EPI point-contact function increases similar to the case of Eliashberg function. The orientational anisotropy of $g_{pc}(\omega)$ is not strong but it is noticeable in passing from the contact axis orientation in the (001) plane to any direction outside this plane (see results for the (111) orientation, figure 5). It is interesting that relativistic effects

are the most essential for the FS topology and electron velocities in this direction, and the $g_{pc}(\omega)$ function taken in this orientation has the most pronounced features at 13 and 23 meV. The same features are also revealed in the EPI transport function, $\alpha^2_{tr}F(\omega)$, calculated in the present work (figure 3) while they were not found in the non-relativistic approach [7]. Thus we may conclude that relativistic effects should be taken into account in order to describe theoretically the fine structure of the EPI spectral function even for relatively light elements. It should be noted that, as in the case of iridium [3] and rhodium [4], the transport and point-contact EPI functions appear to be qualitatively similar in palladium (figure 3).

In general it is evident that the structure of EPI point-contact function is in fact determined by the structure of the phonon spectrum. The suppression of low-energy phonons is due to the structure factor of narrowing; FS anisotropy changes the relative intensity of the peaks in $g_{pc}(\omega)$ compared with $F(\omega)$; the anisotropy of the EPI matrix element mainly affects the EPI point-contact function in the 10–20 meV energy range. All these factors result in the formation of the typical structure of $g_{pc}(\omega)$ with a shoulder at low energies. The calculated position of this shoulder is shifted by 4 meV to higher energies compared with the measured one. This could be due to an inaccurate calculation of the off-symmetry transverse phonon frequencies in the pseudopotential model [13]. At the same time the 23 meV feature found experimentally in this study is also present in the calculated $g_{pc}(\omega)$ function at the same energy, and the positions of the main peaks of the measured and computed EPI functions nearly coincide. Thus we may conclude that the phonon spectrum used here is sufficiently accurate at least for frequencies higher than 12 meV.

It is common practice to use the electron–phonon coupling constant as a quantitative characteristic of the EPI. In the present work we obtain $\lambda = 0.36$ from integration of the Eliashberg function. This value is close to the value of 0.41 obtained in [24] in the Hopfield–McMillan approximation and it is lower than the experimental value derived in [24] from comparison of the calculated and measured cyclotron masses. The reason for this discrepancy pointed out in [24] is connected with the essential role of spin fluctuations in palladium.

5. Conclusion

Our results indicate that the main structure of the point-contact EPI function in palladium originates from the structure of the phonon spectrum, while the ratio of the peak intensities is also determined by the FS topology and by the anisotropy of the EPI. EPI anisotropy explains the formation of a shoulder at the low-energy side of the main peak in point-contact, transport EPI functions and in the Eliashberg function. The point-contact structure factor of narrowing mainly influences the efficiency of low energy phonons in electron–phonon scattering.

Acknowledgments

The authors benefited greatly from fruitful discussions of the present results with Professor O K Andersen, Dr O Jepsen, Professor V V Nemoshkalenko and Professor I K Yanson. One of us (VNA) would like to thank the MPI FKF for the hospitality during his stay in Stuttgart.

References

[1] Krainyukov S N, Khotkevich A V, Yanson I K, Zhalko-Titarenko A V, Antonov V N and Nemoshkalenko V V 1988 *Fiz. Nizk. Temp.* **14** 235 (Engl. Transl. 1988 *Sov. J. Low Temp. Phys.* **14** 127)

[2] Nemoshkalenko V V, Milman V Yu, Zhalko-Titarenko A V, Antonov V N and Shitikov Yu L 1988 *Pis. Zh. Eksp. Teor. Fiz.* **47** 245 (Engl. Transl. 1988 *JETP Lett.* **47** 295)

[3] Krainyukov S N, Khotkevich A V, Yanson I K, Zhalko-Titarenko A V, Antonov V N, Nemoshkalenko V V, Milman V Yu, Shitikov Yu L and Khlopkin M N 1989 *Fiz. Tverd. Tela* **31** 123 (Engl. Transl. 1989 *Sov. Phys.-Solid State* **31** 419)

[4] Zhalko-Titarenko A V, Milman V Yu, Antonov V N, Nemoshkalenko V V, Khotkevich A V and Krainyukov S N 1989 *Metallofizika* **11** N5 23

[5] Miiller A P and Brockhouse B N 1971 *Can. J. Phys.* **49** 704

[6] Pinski F J, Allen P B and Butler W H 1978 *J. Physique Coll.* C6 472

[7] Pinski F J, Allen P B and Butler W H 1981 *Phys. Rev.* B **23** 5080

[8] Caro J, Coehoorn R and de Groot D G 1981 *Solid State Commun.* **39** 267

[9] Caro J 1983 Point-contact spectroscopy of palladium hydride, palladium deuteride and some transition metals *Doctoral Thesis* (Amsterdam: Rodopi)

[10] Schober H R and Dederichs P H 1981 *Phonon Dispersion, Frequency Spectra, and Related Properties of Metallic Elements (Landolt-Bornstein New series)* Group III, vol 13, subvol a, ed K-M Hellwege (Berlin: Springer)

[11] Nemoshkalenko V V, Zhalko-Titarenko A V, Milman V Yu and Antonov V N 1985 *Ukr. Fiz. Zh.* **30** 1372

[12] Antonov V N, Milman V Yu, Nemoshkalenko V V and Zhalko-Titarenko A V 1990 *Z. Phys.* B **79** 223; 1990 *Z. Phys.* B **79** 233

[13] Milman V Yu and Antonov V N 1990 *Solid State Commun.* **76** 1247

[14] Nemoshkalenko V V and Antonov V N 1985 *Methods of Computational Physics in the Solid State Theory. Band Theory of Metals* (in Russian) (Kiev: Naukova Dumka)

[15] Gupta O P 1985 *J. Chem. Phys.* **82** 927

[16] Vrati S C, Rani N, Gupta D K and Gupta H C 1980 *Phys. Lett.* **79A** 342

[17] Daw M S and Hatcher R D 1985 *Solid State Commun.* **56** 697

[18] Yanson I K and Khotkevich A V 1986 *Atlas of Point-Contact Spectra of Electron-Phonon Interaction in Metals* (in Russian) (Kiev: Naukova Dumka)

[19] Kulik I O 1985 *Fiz. Nizk. Temp.* **11** 937 (Engl. Transl. 1985 *Sov. J. Low Temp. Phys.* **11** 516)

[20] Yanson I K, Kulik I O and Batrak A G 1981 *J. Low Temp. Phys.* **42** 527

[21] Kulik I O, Omelyanchuk A N and Shekhter R I 1977 *Fiz. Nizk. Temp.* **3** 1543

[22] Zhalko-Titarenko A V, Antonov V N, Nemoshkalenko V V and John W 1985 *Phys. Status Solidi* **132** K15 (Engl. Transl. 1977 *Sov. J. Low Temp. Phys.* **3** 740)

[23] Pinski F J, Allen P B and Butler W H 1978 *Phys. Rev. Lett.* **41** 431

[24] Antonov V N 1984 *Dokl. Akad. Nauk Ukr.SSR* A **4** 49

[25] Andersen O K 1970 *Phys. Rev.* B **2** 883